pH-Responsive Biocompatible Fluorescent Polymer Nanoparticles Based on Phenylboronic Acid for Intracellular Imaging and Drug Delivery

ARTICLE *in* NANOSCALE · SEPTEMBER 2014

Impact Factor: 7.39 · DOI: 10.1039/C4NR04054F

Nanoscale

PAPER

View Article Online
View Journal | View Issue

Cite this: *Nanoscale*, 2014, **6**, 13701

pH-responsive biocompatible fluorescent polymer nanoparticles based on phenylboronic acid for intracellular imaging and drug delivery†

Shengliang Li,‡[a,b] Kelei Hu,‡[a,c] Weipeng Cao,[a] Yun Sun,[a] Wang Sheng,[c] Feng Li,[b] Yan Wu*[a] and Xing-Jie Liang*[a]

Received 17th July 2014,
Accepted 9th September 2014

DOI: 10.1039/c4nr04054f

www.rsc.org/nanoscale

To address current medical challenges, there is an urgent need to develop drug delivery systems with multiple functions, such as simultaneous stimuli-responsive drug release and real-time imaging. Biocompatible polymers have great potential for constructing smart multifunctional drug-delivery systems through grafting with other functional ligands. More importantly, novel biocompatible polymers with intrinsic fluorescence emission can work as theranostic nanomedicines for real-time imaging and drug delivery. Herein, we developed a highly fluorescent nanoparticle based on a phenylboronic acid-modified poly(lactic acid)–poly(ethyleneimine)(PLA–PEI) copolymer loaded with doxorubicin (Dox) for intracellular imaging and pH-responsive drug delivery. The nanoparticles exhibited superior fluorescence properties, such as fluorescence stability, no blinking and excitation-dependent fluorescence behavior. The Dox-loaded fluorescent nanoparticles showed pH-responsive drug release and were more effective in suppressing the proliferation of MCF-7 cells. In addition, the biocompatible fluorescent nanoparticles could be used as a tool for intracellular imaging and drug delivery, and the process of endosomal escape was traced by real-time imaging. These pH-responsive and biocompatible fluorescent polymer nanoparticles, based on phenylboronic acid, are promising tools for intracellular imaging and drug delivery.

Introduction

Progress in biomaterials research has contributed to promising advances in the construction of intelligent drug delivery systems for nanomedicine.[1,2] Among these nano-materials, biocompatible and biodegradable polymers are the most attractive for biomedical applications because they mostly undergo degradation by hydrolysis or enzymatic activity in the body.[3,4] Moreover, biocompatible polymers can be grafted with other polymers or modified by targeting ligands to construct intelligent multifunctional nanoparticles.[5–8] Despite the intrinsic advantages of such biocompatible polymers, clinical outcomes are still restricted. When these polymers are developed as drug delivery systems, drawbacks are encountered such as drug leakage,[9,10] non-specific targeting effects,[11] difficulties in monitoring cellular events after drug delivery, *etc.*[12,13] Therefore, the design and development of smart drug delivery systems with multiple functions, such as simultaneous stimuli-responsive drug release and real-time imaging, are becoming increasingly urgent. Drug release systems that respond to pH,[14–16] redox conditions,[17,18] light, *etc.*,[19–21] have been developed and widely used in controlled drug delivery. Phenylboronic acid is a key ligand employed in the development of pH-responsive drug delivery systems, and has already been used as the building block to construct stimuli-responsive polymers.[22,23] For instance, Li and coworkers have developed phenylboronic acid-based cross-linked nanoparticles to improve the therapeutic efficiency of Dox and reduce its side effects.[24]

Recently, significant efforts have been focused on developing biocompatible polymers with fluorescence properties for real-time imaging of drug delivery.[25–27] Specifically, fluorescent nanoparticles have gained increasing attention because of their theranostic characteristics. Fluorescent nanoparticles loaded with drugs have been used as *in vitro* and *in vivo* tracers for simultaneous diagnosis and cellular localization of drug delivery systems. However, existing strategies for creating nanoparticles with fluorescence properties have generally focused

[a]*Chinese Academy of Sciences Key Lab for Biological Effects of Nanomaterials and Nanosafety, National Center for Nanoscience and Technology, No. 11, First North Road, Zhongguancun, 100190 Beijing, P.R. China. E-mail: liangxj@nanoctr.cn, wuy@nanoctr.cn*
[b]*Department of Neurobiology and Anatomy, Zhongshan School of Medicine, Sun Yat-sen University, Guangzhou, China*
[c]*College of Life Science and Bioengineering, Beijing University of Technology, No. 100 Pingleyuan, Chaoyang District, Beijing 100124, P.R. China*
† Electronic supplementary information (ESI) available. See DOI: 10.1039/c4nr04054f
‡ These authors contributed equally to this work.

on encapsulation or conjugation of fluorescent ligands, such as organic dyes,[28,29] quantum dots (QDs),[30,31] or carbon dots.[32] Unfortunately, these strategies often change the size of the original nanoparticle, increasing the cytotoxicity and decreasing the drug loading capacity. Furthermore, fluorescence quenching and leakage of the dye are inevitable, and these drawbacks influence the imaging quality and interfere with the quality of tracing.[33,34]

Therefore, it is important to design and develop novel biocompatible polymers or nanoparticles with intrinsic fluorescence for real-time tracking of the drug delivery system. Recently, a series of biocompatible polymers with intrinsic fluorescence properties were developed and used as vectors for drug or gene delivery. For example, Yang and co-workers designed a series of fluorescent amphiphilic polymers which were used as Dox vectors for simultaneous diagnosis and therapy applications.[35,36] Meanwhile, Wang and co-workers developed a gene vector based on a highly fluorescent cationic conjugated polyelectrolyte, which was used for real-time tracking of the location of gene delivery and DNA transfection.[37] Accompanied by the latest developments in nanomedicine, fluorescent polymers have huge potential in the development of tools for diagnosis and therapy.

We have previously developed smart fluorescent nanoparticles made from a biocompatible amphiphilic PLA–PEI copolymer with high quantum yield. We demonstrated the therapeutic efficiency of paclitaxel-loaded nanoparticles, which could be used as theranostic tools *in vitro* and *in vivo*.[38] Herein, we developed smart nanoparticles for Dox delivery based on the fluorescence of the PLA–PEI copolymer and the pH-responsiveness of phenylboronic acid. As shown in Fig. 1, these smart fluorescent boronate nanoparticles (FBNPs) show high fluorescence emission, and the release of encapsulated Dox is controlled by pH to minimize premature escape of the drug. We demonstrated here that pH-responsive fluorescent nanoparticles based on phenylboronic acid allow spatial visualization of the drug delivery process and heighten the anticancer therapy effect.

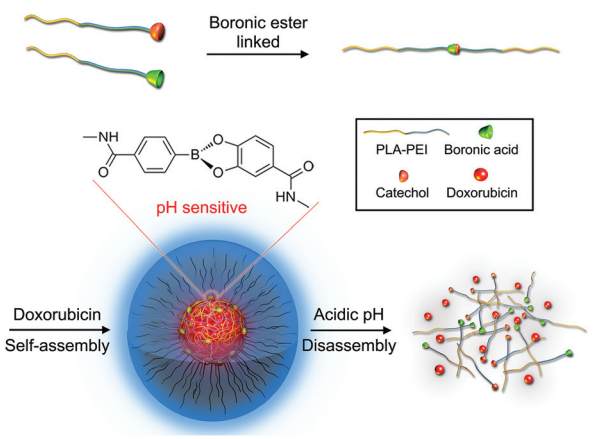

Fig. 1 Schematic illustration of the formulation of FBNPs-Dox and pH-responsive Dox release.

Results and discussion

Synthesis and functionalization of copolymers

We here describe the successful synthesis and functionalization of novel fluorescent nanoparticles for pH-responsive drug delivery. The amphiphilic PLA–PEI copolymer was first synthesized by grafting hydrophilic PEI with hydrophobic PLA using a one-step ring-opening polymerization method as previously described with some modifications.[38] In order to achieve pH-responsive drug release, the PLA–PEI copolymer was subsequently coupled with 3,4-dihydroxybenzoic acid (DHB) and 4-carboxyphenylboronic acid pinacol ester (CPB) using EDC/NHS chemistry (Fig. S1†). The chemical structures of these as-synthesised polymers were further confirmed by FT-IR, ^{1}H NMR and ^{13}C NMR. As shown in FT-IR spectra (Fig. 2a, b, S2†), the absorption peaks at ~1652 and ~1659 cm^{-1} resulted from the amide I bands and the peaks at ~1545 and ~1520 cm^{-1} from the amide II bands in PLA–PEI–CPB and PLA–PEI–DHB, respectively, and the slight absorption peaks at ~1502 and ~1610 cm^{-1} were ascribed to the skeletal vibration of the benzene ring in CPB and DHB, respectively. In ^{1}H NMR analysis (Fig. 2c, d, S3†), the signals at ~1.46 and ~5.20 ppm corresponded to the protons of the methyl (3H, –C**H**$_3$) and methine (1H, –C**H**–) in PLA, and the signals at ~2.73 and ~2.89 ppm were attributed to the protons of methylene (2H, –C**H**$_2$–CH$_2$–NH$_2$) and (2H, –CH$_2$–C**H**$_2$–NH$_2$), respectively. In addition, the signals at ~6–8 ppm of two spectra could be assigned to the protons of the aromatic ring moiety in PLA–PEI–DHB and PLA–PEI–CPB. Together, these results demonstrated the successful synthesis of the PLA–PEI copolymer and its functionalized derivatives PLA–PEI–CPB and PLA–PEI–DHB. The molar ratio of CPB, PEI and PLA was 1 : 4.12 : 118.9 in the polymer PLA–PEI–CPB, and the molar ratio of DHB, PEI and PLA 1 : 3.65 : 134.5. The molecular weight of the

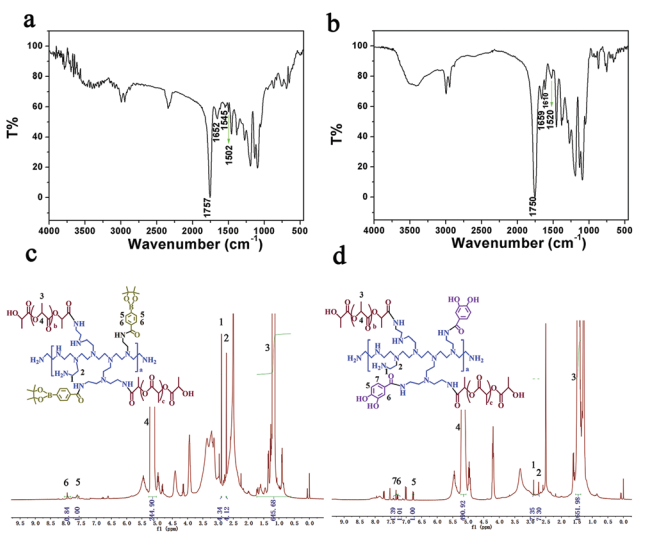

Fig. 2 Characterization of the PLA–PEI copolymer and its functionalized derivatives. FT-IR spectra of PLA–PEI–CPB (a), PLA–PEI–DHB (b), and ^{1}H NMR spectra of PLA–PEI–CPB (c), PLA–PEI–DHB (d).

PLA–PEI–DHB copolymer was 123 kDa and the polydispersity (M_w/M_n) was 1.50, while the molecular weight of PLA–PEI–CPB was 117 kDa (M_w/M_n = 1.51).

Characterization of Dox-loaded nanoparticles

Owing to the fact that pH-responsive boronate esters can be formed through the interaction of boronic acids and diols, there has been increasing interest in using boronic acids as platforms to design stimuli-responsive drug delivery systems. Herein, we described the successful fabrication of novel pH-responsive fluorescent boronate nanoparticles for drug delivery based on the self-assembly and crosslinking of boronic acid-containing polymers (PLA–PEI–CPB) and catechol-containing polymers (PLA–PEI–DHB). The FBNPs were then constructed by a modified double emulsion technique as previously reported.[39] To obtain nanoparticles with small size and high encapsulation efficiency, we studied the influences of various parameters (the concentration of polyvinyl alcohol (PVA), the mass of copolymers and Dox) on encapsulation efficiency (EE), drug-loading content (LC), particle size, polydispersity index (PDI) and zeta potential of the nanoparticles as shown in Table 1. We used the optimum preparation conditions for the following experiments. The prepared blank FBNPs were well dispersed with a typical spherical shape and a size around 100 nm (Fig. 3a). The hydrodynamic size of the nanoparticles in phosphate buffer solution was 225.3 ± 4.2 nm by dynamic light scattering (DLS) (Fig. 3b). Dox-loaded FBNPs were slightly larger than blank FBNPs (245.1 ± 3.7 nm), attributable to the encapsulation of Dox (Fig. 3c,d). The size of nanoparticles obtained by DLS showed the hydrodynamic diameter of nanoparticles swelling in aqueous solution, whereas that obtained by TEM was the diameter of dried nanoparticles. Therefore, the size obtained by DLS was larger than that obtained by TEM. The encapsulation efficiency and drug-loading content of Dox-loaded FBNPs were 57.6 ± 3.6% and 5.45 ± 0.23%, respectively. The zeta potential of Dox-loaded FBNPs was 10.7 ± 1.5 mV. The reason for the low zeta potential is that the amino groups of the PEI in the nanoparticles had partly reacted with PLA, DHB and CPB.

Fluorescence characterization of cross-linked NPs

Our previous research has shown that PLA–PEI nanoparticles exhibit extraordinarily bright and colorful fluorescence.[38] The

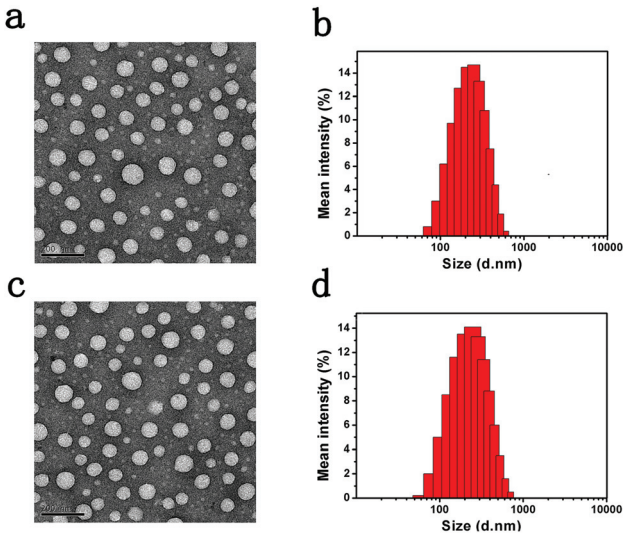

Fig. 3 TEM and DLS characterization of blank FBNPs (a,b) and Dox-loaded FBNPs (c,d). Scale bar: 200 nm.

fluorescence characteristics of FBNPs were further analyzed by fluorescence spectrophotometry. As shown in Fig. 4a, the UV-Vis spectra of FBNPs exhibited fairly broad absorption ranging from 200 to 700 nm, with no obvious peak. Moreover, the emission spectra of the FBNPs were also generally broad and were sensitive to the excitation wavelength. The emission peak shifted from 450 nm to 850 nm with the fluorescence emission intensity decreasing markedly when the FBNP solution was excited at wavelengths from 360 to 540 nm. The fluorescence quantum yield (QY) of the FBNPs at an emission wavelength of 450 nm was as high as 22.6% using rhodamine B as the reference (Table S1†). This is slightly lower than the 31% QY of PLA–PEI nanoparticles. We then investigated the fluorescence lifetime of the FBNPs in order to understand the mechanism underlying the fluorescence enhancement (Fig. 4b). The FBNPs possess a characteristic multi-exponential fluorescence decay that fitted well with two exponential functions, with lifetimes (fractional weights) of 4.48 ns (59.0%) and 1.15 ns (41.0%), and the mean fluorescence lifetime of the FBNPs was 3.12 ns. In order to test their suitability for imaging applications, we further checked the photostability of FBNPs. As shown in Fig. 4c, the FBNPs showed excellent

Table 1 The effects of formulation parameters on drug-loading content and encapsulation efficiency (n = 3)

Sample number	Copolymer (mg)	Dox (mg)	PVA (w/v)	EE (%)	LC (%)	Size (nm)	PDI	Zeta (mV)
Blank	40	0	2	—	—	225.3 ± 4.2	0.118 ± 0.024	10.4 ± 0.2
1	10	1	2	16.7 ± 1.5	5.11 ± 0.32	221.3 ± 4.2	0.116 ± 0.008	6.2 ± 0.9
2	20	1	2	32.5 ± 2.7	4.83 ± 0.14	256.4 ± 5.2	0.176 ± 0.021	8.9 ± 0.3
3	80	1	2	71.3 ± 4.5	2.42 ± 0.21	293.6 ± 4.3	0.186 ± 0.006	14.5 ± 0.8
4	40	0.5	2	69.5 ± 3.3	2.24 ± 0.24	239.1 ± 2.8	0.124 ± 0.013	10.1 ± 0.5
5	40	2	2	36.7 ± 2.2	4.39 ± 0.22	284.5 ± 3.6	0.155 ± 0.002	11.8 ± 1.2
6	40	1	0.5	41.2 ± 1.4	2.78 ± 0.11	301.4 ± 3.9	0.209 ± 0.012	9.4 ± 1.2
7	40	1	1	44.3 ± 2.1	3.30 ± 0.18	272.3 ± 3.2	0.173 ± 0.009	9.5 ± 2.1
8	40	1	2	57.6 ± 3.6	5.45 ± 0.23	245.1 ± 3.7	0.096 ± 0.002	10.7 ± 1.5
9	40	1	4	50.8 ± 6.2	4.06 ± 0.16	226.7 ± 4.6	0.192 ± 0.014	11.2 ± 1.1

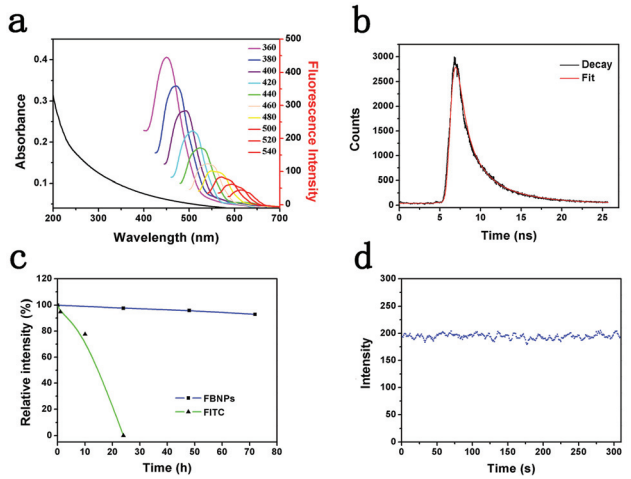

Fig. 4 (a) UV-Vis spectrum (black line) and fluorescence spectra of FBNPs (with excitation wavelengths in 20 nm increments from 360 nm). (b) The fluorescence lifetime parameters of FBNPs. (c) Photostability of FBNPs and fluorescein (FITC) under a high-brightness cold light source (the CRi Maestro *in vivo* imaging system). (d) Time-dependent fluorescence behavior of FBNPs under laser irradiation.

photostability, and their fluorescence stayed at more than 90% even after continuous excitation with a 300 W Xe lamp for 72 h, while the fluorescence of fluorescein was quenched after 20 h under the same cold light source. The FBNPs were found to be extraordinarily photostable, emitting fluorescence even after being scanned three hundred times under laser excitation at 405 nm (Fig. 4d). The fluorescence emitted by FBNPs was constant, with no fluorescence blinking effect, while the blinking effect has been a major hurdle preventing wider application of quantum dots and noble metal nanocrystals (Fig. 4d). These results demonstrated that FBNPs, with their unique fluorescence properties, are promising probes for intracellular imaging and drug delivery.

In vitro drug release studies

Controlled drug release is very important for drug delivery systems. The pH of tumor tissue is much lower than normal because of lactic acid produced due to hypoxia and acidic intracellular organelles.[40,41] The pH-dependent nanocarriers can avoid premature drug release at physiological pH values (pH 7.4) in blood circulation but can be activated to release drugs at the acidic tumor microenvironment or in the acidic cellular compartments upon uptake into tumor cells. Therefore, pH-responsive properties are important for the development of smart nanomedicines. The Dox release profile from FBNPs-Dox and non-crosslinked nanoparticles (NCNPs) derived from PLA–PEI were evaluated by dialysis. As shown in Fig. 5, NCNPs-Dox possessed a similar drug release profile at pH 7.4 and pH 5.4. Nevertheless, Dox was hardly released from FBNPs at pH 7.4 during the initial 4 h. When the pH of the medium was adjusted to 5.4 at 4 h, there was a burst of drug release from the FBNPs, indicating that the FBNPs-Dox has a pH-sensitive release profile. These pH sensitivity properties

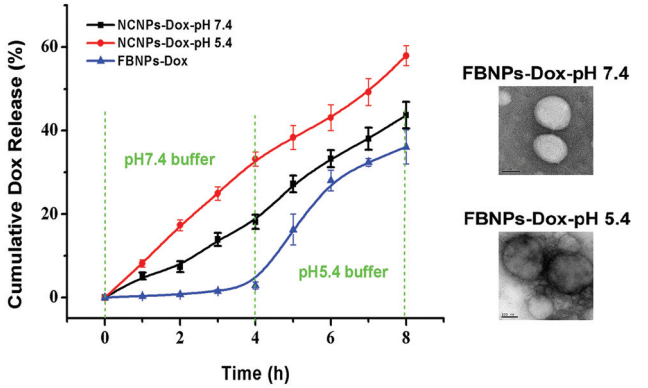

Fig. 5 *In vitro* drug release studies of NCNPs-Dox and FBNPs-Dox at different pH values. Inset: TEM imaging of the pH-sensitive FBNPs at pH 7.4 and 5.4 (scale bars: 50 nm, 100 nm, respectively).

may benefit the release of Dox when drug-loaded FBNPs enter the tumor microenvironment, and the leakage of FBNPs-Dox would be minimized during blood circulation *in vivo*. We also investigated the change in size and morphology of the pH-sensitive FBNPs at different pH (7.4, 5.4) using TEM imaging. As shown in Fig. 5, the nanoparticles undergo a significant size increase and morphology change at pH 5.4. The FBNPs disintegrated and formed large aggregated structures. This result further verified the pH-sensitive release capacity of the smart FBNPs-based delivery system.

Cytotoxicity of Dox-loaded FBNPs

Next, the *in vitro* anti-cancer effect of Dox-loaded NCNPs, Dox loaded FBNPs and free Dox towards MCF-7 breast cancer cells after 24 h treatment was evaluated by MTT assay. As shown in Fig. 6, FBNPs-Dox was more effective in suppressing the proliferation of MCF-7 cells than NCNPs-Dox and free Dox at the same concentration, while the cytotoxicity of NCNPs-Dox was similar to that of free Dox. This may be due to the pH-responsive properties of the FBNPs, which are modified by phenylboronic acid. These results demonstrated that the pH-responsive FBNPs-Dox may potentially be developed as a smart nanomedicine. More importantly, as shown in Fig. S5 and S6,†

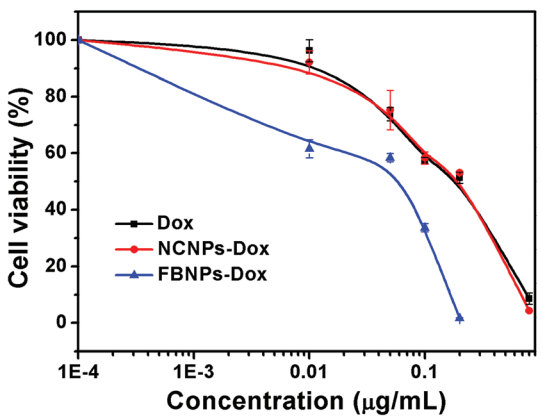

Fig. 6 *In vitro* cytotoxicity of free Dox, NCNPs-Dox and FBNPs-Dox.

pH-responsive FBNPs-Dox was also more toxic to multidrug-resistant MCF-7R cells than free Dox. FBNPs-Dox showed a lower IC_{50} (about 7.6 μM) than free DOX (about 24.3 μM) and NCNPs-Dox (about 10.4 μM). These results indicated that the pH-responsive FBNPs-Dox nanoparticles have a better anti-tumor effect on MCF-7R compared with free Dox.

Cellular uptake and intracellular localization of Dox loaded FBNPs

Owing to the high fluorescence emission of FBNPs, we evaluated the possibility of using the FBNPs as a fluorescent probe for tracing the cellular uptake and intracellular kinetics of the drug delivery system in real time *via* confocal laser scanning microscopy (CLSM). We first investigated the cellular uptake of Dox-loaded FBNPs by MCF-7 cells using CLSM (Fig. 7). MCF-7 cells were incubated with free Dox, blank FBNPs and FBNPs-Dox at 37 °C for 0.5 or 3 h with the Dox concentration of 10 μg mL^{-1}. CLSM imaging revealed that the blue fluorescence derived from FBNPs was clearly visible in the cytoplasm after 0.5 h treatment. This result showed that FBNPs could easily access the intracellular environment of MCF-7 cells. After 0.5 h treatment, the red fluorescence from Dox delivered by FBNPs was much stronger than that from free Dox (Fig. 7). This may result from different uptake pathways. After 3 h treatment, the CLSM results demonstrated that the cellular uptake of FBNPs-Dox was similar to free Dox. We also found that the cellular uptake of FBNPs-Dox increased as the incubation time was extended from 0.5 to 3 h.

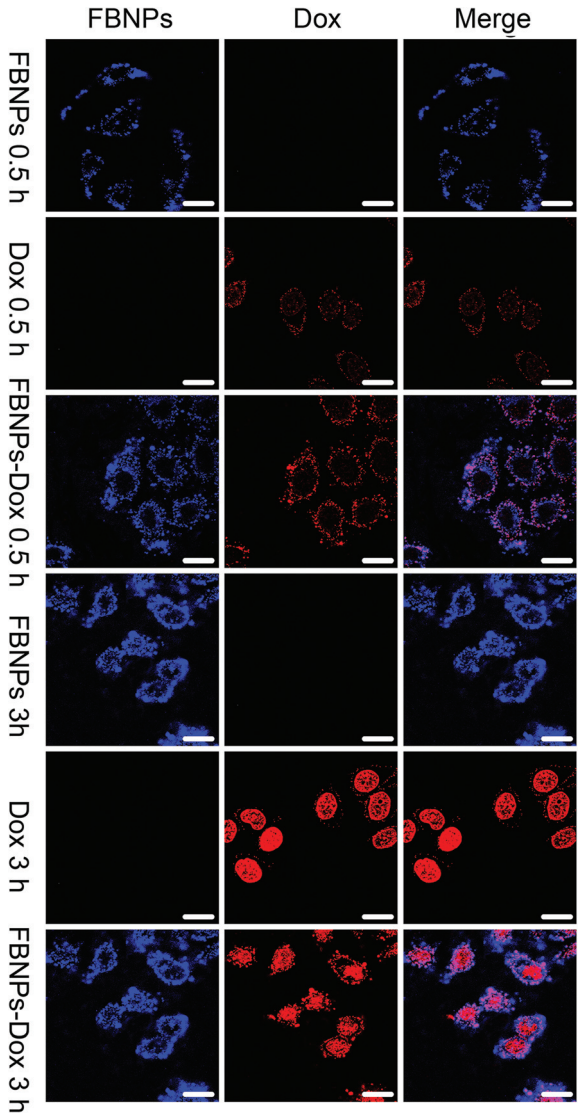

Fig. 7 Cellular imaging of MCF-7 cells incubated with free Dox, FBNPs and FBNPs-Dox for various times. Scale bar: 10 μm.

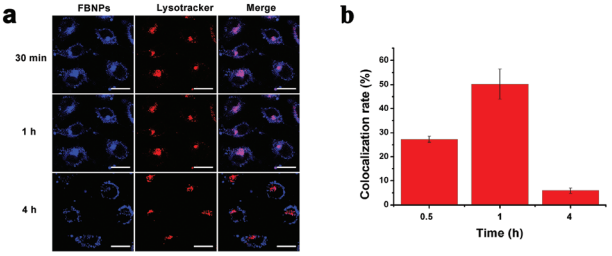

Fig. 8 Colocalization between FBNPs and endosomes. CLSM images (a) and the corresponding histogram (b). Lysosomes were stained with Lysotracker Deep Red (Molecular Probes, USA) for 30 min. Scale bar: 10 μm.

Endosomal escape is very important for drug delivery because most nanoparticles entered cells by endocytosis, and were then stored in endosome or lysosome. If these intracellular nanoparticles cannot escape from the endosome or lysosome, the drug loading nanoparticles cannot release the encapsulated drug into the cytoplasm or nucleus for tumor therapy. Therefore, we further investigated the distribution and colocalization of FBNPs and endosomes by CLSM imaging at various time points. As shown in Fig. 8, the blue fluorescence of FBNPs co-localized with the endosomes (labeled with Lysotracker Deep Red) after 0.5 h and 1 h treatment. However, the blue fluorescence of FBNPs was separate from the endosomes at 4 h. The CLSM imaging results indicated that the FBNPs could effectively escape from the endosomes into the cytoplasm, presumably as a result of the proton sponge effect of the PEI in the FBNPs.

We next evaluated the potentiality of FBNPs as fluorescent probes for *in vivo* imaging. The FBNPs were administered to MCF-7 tumor-bearing mice through intratumor injection. As shown in Fig. S7,† a significant fluorescence of the FBNPs was observed in the interior of the tumor using green laser light excitation, and no fluorescence signal appeared in other parts of mice. These results demonstrated that the FBNPs possess the potency for *in vivo* imaging.

Biocompatibility of FBNPs

The biocompatibility of FBNPs was investigated by MTT assay in human breast cancer MCF-7 cells (Fig. 9a). FBNPs were less cytotoxic than NCNPs. Although the cytotoxicity of the FBNPs increased slightly with increasing concentration, the concentrations of FBNPs used in cell research were significantly lower than the concentrations tested by MTT assay. For hemolysis

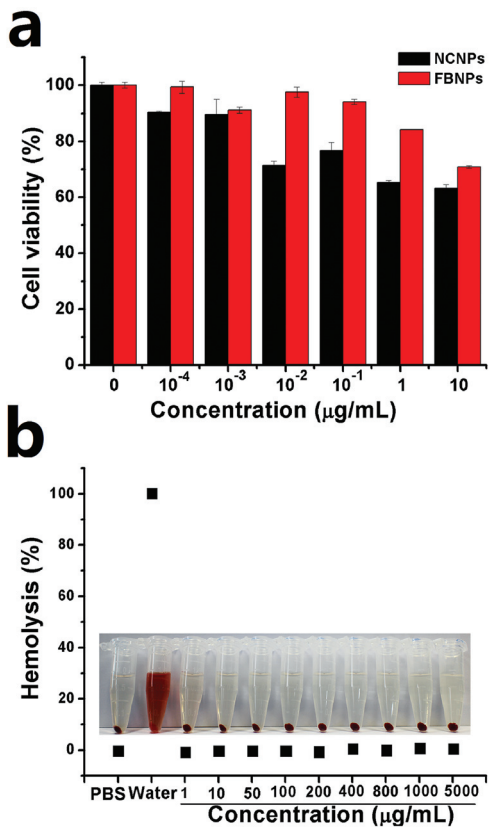

Fig. 9 (a) Cytotoxicity of MCF-7 cells incubated with NCNPs and FBNPs at various concentrations. (b) Hemolysis assay with different concentrations of FBNPs (negative control: phosphate buffer solution; positive control: water).

analysis, if erythrocytes are lysed, hemoglobin will be released from erythrocytes and the supernatant will appear red. Meanwhile, the hemoglobin in the supernatant can be measured by measuring the absorbance. Furthermore, hemolysis assay was performed to check the hemocompatibility of the FBNPs. As shown in Fig. 9b, no hemolysis of red blood cells was caused by the FBNPs, even at a concentration of 5000 μg mL^{-1}, indicating favorable blood compatibility. Thus, the cellular toxicity test and hemolysis assay confirmed the biocompatibility of the FBNPs.

Conclusions

In conclusion, we developed a highly fluorescence emissive nanoparticle loaded with Dox for intracellular imaging and pH-responsive drug delivery. The FBNPs exhibited fluorescence stability, excitation-dependent fluorescence behavior and no blinking. More importantly, the Dox-loaded phenylboronic acid-modified fluorescent nanoparticles showed a pH-responsive drug release pattern. This work showed that Dox-loaded FBNPs were more effective in suppressing the growth of MCF-7 cells than free Dox and Dox-loaded NCNPs. Moreover, the biocompatible fluorescent nanoparticles can escape from endosomes and are suitable for use as a tool for intracellular imaging and drug delivery. In summary, this pH-responsive biocompatible fluorescent polymer nanoparticle, based on phenylboronic acid, is a promising candidate for progressing pH-responsive drug delivery systems.

Experimental section

Materials and cell lines

Branched polyethyleneimine (PEI, 25 kDa) was obtained from Sigma-Aldrich (St. Louis, MO, USA). D,L-lactide (DLLA), 3,4-dihydroxybenzoic acid (DHB), 4-carboxyphenylboronic acid pinacol ester (CPB), *N*-hydroxysuccinimide (NHS) and 1-ethyl-3-(3-dimethylaminopropyl)-carbodiimide (EDC) were obtained from Alfa Aesar (Ward Hill, MA, USA). Doxorubicin hydrochloride salt was purchased from Beijing HuaFeng Unite Co., Ltd (China). 3-(4,5-dimethylthiazol-2-yl)-2,5- diphenyltetrazolium bromide (MTT) was purchased from Sigma (Japan). Human breast adenocarcinoma (MCF-7) cells were purchased from the American Type Culture Collection (ATCC; Manassas, VA, USA). Unless specified, all the commercial products were used without further purification.

Synthesis and conjugation of PLA–PEI

The PLA–PEI copolymer was synthesized according to our previous method[38] with some modifications as follows: predehydrated DLLA and PEI (mass ratio 60 : 1) were reacted in dimethylsulfoxide at 86 °C with constant stirring under nitrogen for 12 h. This solution was then poured into ice-cold water and the precipitate was collected after being thoroughly washed with distilled water. The brown copolymer was dried under vacuum at room temperature for 48 h.

PLA–PEI–DHB and PLA–PEI–CPB were synthesized by linking DHB and CPB to PLA–PEI. First, the carboxyl groups of DHB and CPB were activated by excess NHS in the presence of EDC in dimethylsulfoxide (20 mL). PLA–PEI–NH_2 was then added to the solutions of active DHB–NHS or CPB–NHS and reacted for 2 h. The final products were dialyzed against distilled water for 24 h to remove unreacted reagents. The resulting PLA–PEI–DHB and PLA–PEI–CPB copolymers were lyophilized and used without further treatment.

The chemical structures of the copolymers were characterized by Fourier-transform infrared spectroscopy (FT-IR) and nuclear magnetic resonance (^{1}H NMR). For FT-IR analysis, copolymers and KBr (mass ratio: 1 : 50) were mixed to make transparent slices and analyzed on a Fourier-transform infrared instrument (Perkin-Elmer, Fremont, CA, USA). For ^{1}H NMR analysis, the samples were dissolved in DMSO-d_6 and analyzed using a Bruker AVANCE 400 NMR spectrometer (Billerica, MA, USA).

Preparation and characterization of Dox-loaded nanoparticles

Dox-loaded nanoparticles and blank nanoparticles were prepared by the double emulsion (W/O/W) method with minor modification. Briefly, equal masses of PLA–PEI–DHB and

PLA–PEI–CPB copolymers were first dissolved in 2 mL dichloromethane and 400 μL Dox aqueous solution or distilled water (blank nanoparticles) was added to the copolymer solution. The mixture was emulsified by sonication for 1 min at 5 W in an ice bath. Then 5 mL of PVA solution (0.5–4% (w/v)) was added and sonicated for 5 min at 20 W to make a W/O/W emulsion. After vacuum evaporation of dichloromethane, the FBNPs-Dox and blank FBNPs were collected by centrifugation at 15 000 rpm for 10 min at room temperature and washed three times with distilled water before lyophilization.

The particle size distribution, polydispersity index and zeta potential of the blank FBNPs and FBNPs-Dox in phosphate buffer solution (PBS) of different pH values were determined by dynamic light scattering (DLS) with a ZetaSizer Nano series Nano-ZS (Malvern Instruments Ltd, Malvern, UK). The morphology of the nanoparticles was determined using an FEI Tecnai F20 U-TWIN electron microscope (TEM) (FEI Company, Philips, Netherlands) after negative staining with uranyl acetate. The UV-Vis spectra of the FBNP solution were obtained using a UV-Vis spectrophotometer (Perkin Elmer Lambda 850). The fluorescence spectra of the FBNP solution were detected using a LS-55 fluorescence spectrometer (Perkin-Elmer, Fremont, CA, USA) and the fluorescence quantum yield was determined by using quinolone sulfate as the reference.

Encapsulation efficiency and loading content of Dox-loaded nanoparticles

The drug encapsulation efficiency and loading content of Dox-loaded nanoparticles were measured by UV-Vis spectrophotometry (Perkin Elmer Lambda 850). The free Dox recovered in the final aqueous phase was measured at 480 nm. The Dox loading content and encapsulation efficiency were defined as follows:

$$\text{Loading content } (\%) = (W_0 - W_t)/W_s \times 100\%$$

$$\text{Encapsulation efficiency } (\%) = (W_0 - W_t)/W_0 \times 100\%$$

W_0 is the weight of initial Dox and W_t is the total amount of Dox detected in supernatant after centrifuging twice. W_s is the weight of Dox-loaded nanoparticles after lyophilization. Each sample was assayed in triplicate.

In vitro drug release

Typically, 20 mg Dox-loaded nanoparticles were dispersed in 5 mL deionized water and then transferred into a dialysis bag (MWCO: 3500 Da). The dialysis bag was then incubated in 40 mL of PBS at pH 7.4 or 5.4 at 37 °C and stirred at a constant rate of 150 rpm. At given intervals, 0.5 mL of the medium was extracted and the Dox concentration was measured by UV-Vis spectrophotometry as described above. Afterwards, 0.5 mL of fresh PBS at the same pH was added to the dialysis bag. In the assessment of drug release behavior, the cumulative amount of released drug was calculated, and the percentage of drug released from the nanoparticles was plotted against time.

Cytotoxicity assays

MCF-7 cells were seeded at a density of 5×10^3 cells per well in 96-well plates in DMEM medium and incubated overnight. The medium was then replaced with 100 μl of medium containing various equivalent concentrations of blank nanoparticles, free-Dox and Dox-loaded nanoparticles. After 24 h incubation, the medium was replaced with 100 μl 0.5 mg ml^{-1} MTT and incubated for 3 h. The MTT solution was then replaced with 150 μl DMSO solution. The absorbance was measured at 570 nm with a reference wavelength of 630 nm using an Infinite M200 microplate reader (Tecan, Durham, USA). Untreated cells in medium were used as controls. All data are presented as mean ± SD in triplicate compared to the OD values of untreated cells.

Doxorubicin uptake

Cellular uptake of Dox-loaded FBNPs was investigated by confocal imaging analysis. For confocal imaging, MCF-7 cells were seeded into 35 mm dishes and incubated at 37 °C for 24 h. Cells were then incubated with free Dox, blank FBNPs and FBNPs-Dox at a final concentration of 10 μg ml^{-1} for 0.5 h and 4 h at 37 °C. Finally, the samples were labeled using a UltraView VoX spinning disc confocal microscope (PerkinElmer Inc., USA). The excitation wavelengths were 405 and 488 nm.

Subcellular localization of FBNPs

For observing the subcellular localization of FBNPs, MCF-7 cells were seeded into 35 mm glass dishes and incubated at 37 °C for 24 h, then cultured with blank nanoparticles at a concentration of 10 μg ml^{-1} for 1–4 h at 37 °C. Endosomes and lysosomes were then labeled by Lysotracker Deep Red and the cells were imaged using a UltraView VoX spinning disc confocal microscope (PerkinElmer Inc., USA).

Hemolysis assay

Red blood cells (RBCs) were collected from 800 μl of freshly-drawn whole blood by centrifuging at 10 000*g* for 5 min, then washed three times with PBS. RBCs were suspended in 10 ml PBS, and 0.5 ml of the suspension was added to 0.5 ml of empty nanoparticles dissolved in PBS at final concentrations of 1, 10, 50, 100, 200, 400, 800, 1000 and 5000 μg ml^{-1}. Meanwhile, 0.5 ml of RBC suspension was incubated with 0.5 ml PBS and water as the negative control and positive control, respectively. The samples were vortexed briefly, left at room temperature for 3 h, and then centrifuged at 10 000*g* for 5 min. 100 μl of supernatant was transferred to a 96-well plate and the absorbance value at 577 nm was measured with a reference wavelength of 655 nm. The percentage of hemolysis was calculated as follows:

$$\text{Hemolysis } \% = \frac{\text{sample absorbance} - \text{negative control}}{\text{positive control} - \text{negative control}} \times 100\%$$

Statistical analysis

All data are presented as mean ± standard deviation (SD). The *t*-test was used to evaluate significant differences between

groups according to Bonferroni's post-test. $p < 0.05$ was considered to be statistically significant.

Acknowledgements

This work was supported by the Chinese Natural Science Foundation project (no. 81171455, 81272453, 81271476, and 31170873), a National Distinguished Young Scholars grant (31225009) from the National Natural Science Foundation of China, the National Key Basic Research Program of China (2009CB930200), the Chinese Academy of Sciences (CAS) "Hundred Talents Program" (07165111ZX), the CAS Knowledge Innovation Program and the State High-Tech Development Plan (2012AA020804).

Notes and references

1 T. M. Allen and P. R. Cullis, Drug delivery systems: entering the mainstream, *Science*, 2004, **303**, 1818.
2 D. A. LaVan, T. McGuire and R. Langer, Small-scale systems for *in vivo* drug delivery, *Nat. Biotechnol.*, 2003, **21**, 1184.
3 K. Kataoka, A. Harada and Y. Nagasaki, Block copolymer micelles for drug delivery: design, characterization and biological significance, *Adv. Drug Delivery Rev.*, 2001, **47**, 113.
4 B. Jeong, Y. H. Bae, D. S. Lee and S. W. Kim, Biodegradable block copolymers as injectable drug-delivery systems, *Nature*, 1997, **388**, 860.
5 N. Nasongkla, E. Bey, J. Ren, H. Ai, C. Khemtong, J. S. Guthi, S. F. Chin, A. D. Sherry, D. A. Boothman and J. Gao, Multifunctional polymeric micelles as cancer-targeted, MRI-ultrasensitive drug delivery systems, *Nano Lett.*, 2006, **6**, 2427.
6 X. Li, Y. Qian, T. Liu, X. Hu, G. Zhang, Y. You and S. Liu, Amphiphilic multiarm star block copolymer-based multifunctional unimolecular micelles for cancer targeted drug delivery and MR imaging, *Biomaterials*, 2011, **32**, 6595.
7 Y. Liu, L. Feng, T. Liu, L. Zhang, Y. Yao, D. Yu, L. Wang and N. Zhang, Multifunctional pH-sensitive polymeric nanoparticles for theranostics evaluated experimentally in cancer, *Nanoscale*, 2014, **6**, 3231.
8 E. Blanco, C. W. Kessinger, B. D. Sumer and J. Gao, Multifunctional micellar nanomedicine for cancer therapy, *Exp. Biol. Med.*, 2009, **234**, 123.
9 Q. Xu, Y. Tanaka and J. T. Czernuszka, Encapsulation and release of a hydrophobic drug from hydroxyapatite coated liposomes, *Biomaterials*, 2007, **28**, 2687.
10 T. J. Evjen, E. A. Nilssen, S. Rögnvaldsson, M. Brandl and S. L. Fossheim, Distearoylphosphatidylethanolamine-based liposomes for ultrasound-mediated drug delivery, *Eur. J. Pharm. Biopharm.*, 2010, **75**, 327.
11 S. Cai, Y. Xie, N. M. Davies, M. S. Cohen and M. L. Forrest, Pharmacokinetics and disposition of a localized lymphatic polymeric hyaluronan conjugate of cisplatin in rodents, *J. Pharm. Sci.*, 2010, **99**, 2664.
12 J. M. Chan, L. Zhang, K. P. Yuet, G. Liao, J. W. Rhee, R. Langer and O. C. Farokhzad, PLGA-lecithin-PEG core-shell nanoparticles for controlled drug delivery, *Biomaterials*, 2009, **30**, 1627.
13 O. M. Koo, I. Rubinstein and H. Onyuksel, Role of nanotechnology in targeted drug delivery and imaging: a concise review, *Nanomedicine*, 2005, **1**, 193.
14 X. Yang, J. J. Grailer, I. J. Rowland, A. Javadi, S. A. Hurley, V. Z. Matson, D. A. Steeber and S. Gong, Multifunctional stable and pH-responsive polymer vesicles formed by heterofunctional triblock copolymer for targeted anticancer drug delivery and ultrasensitive MR imaging, *ACS Nano*, 2010, **4**, 6805.
15 J. Su, F. Chen, V. L. Cryns and P. B. Messersmith, Catechol polymers for pH-responsive, targeted drug delivery to cancer cells, *J. Am. Chem. Soc.*, 2011, **133**, 11850.
16 M. Krämer, J. F. Stumbé, H. Türk, S. Krause, A. Komp, L. Delineau, S. Prokhorova, H. Kautz and R. Haag, pH-responsive molecular nanocarriers based on dendritic core-shell architectures, *Angew. Chem., Int. Ed.*, 2002, **41**, 4252.
17 Z. Luo, K. Cai, Y. Hu, L. Zhao, P. Liu, L. Duan and W. Yang, Mesoporous silica nanoparticles end-capped with collagen: redox-responsive nanoreservoirs for targeted drug delivery, *Angew. Chem., Int. Ed.*, 2011, **50**, 640.
18 Q. Zhang, N. R. Ko and J. K. Oh, Recent advances in stimuli-responsive degradable block copolymer micelles: synthesis and controlled drug delivery applications, *Chem. Commun.*, 2012, **48**, 7542.
19 K. Peng, I. Tomatsu and A. Kros, Light controlled protein release from a supramolecular hydrogel, *Chem. Commun.*, 2010, **46**, 4094.
20 S. Murdan, Electro-responsive drug delivery from hydrogels, *J. Controlled Release*, 2003, **92**, 1.
21 P. Yang, S. Gai and J. Lin, Functionalized mesoporous silica materials for controlled drug delivery, *Chem. Soc. Rev.*, 2012, **41**, 3679.
22 Z. Luo, K. Cai, Y. Hu, B. Zhang and D. Xu, Cell-specific intracellular anticancer drug delivery from mesoporous silica nanoparticles with pH sensitivity, *Adv. Healthc. Mater.*, 2012, **1**, 321.
23 M. Naito, T. Ishii, A. Matsumoto, K. Miyata, Y. Miyahara and K. Kataoka, A phenylboronate-functionalized polyion complex micelle for ATP-triggered release of siRNA, *Angew. Chem., Int. Ed.*, 2012, **51**, 10751.
24 Y. Li, W. Xiao, K. Xiao, L. Berti, J. Luo, H. P. Tseng, G. Fung and K. S. Lam, Well-defined, reversible boronate cross-linked nanocarriers for targeted drug delivery in response to acidic pH values and cis-diols, *Angew. Chem., Int. Ed.*, 2012, **51**, 2864.
25 P. Yang, S. Huang, D. Kong, J. Lin and H. Fu, Luminescence functionalization of SBA-15 by YVO4:Eu^{3+} as a novel drug delivery system, *Inorg. Chem.*, 2007, **46**, 3203.
26 J. M. Bryson, K. M. Fichter, W. J. Chu, J. H. Lee, J. Li, L. A. Madsen, P. M. McLendon and T. M. Reineke, Polymer beacons for luminescence and magnetic resonance

imaging of DNA delivery, *Proc. Natl. Acad. Sci. U. S. A.*, 2009, **106**, 16913.

27 W. Wang, D. Cheng, F. Gong, X. Miao and X. Shuai, Design of multifunctional micelle for tumor-targeted intracellular drug release and fluorescent imaging, *Adv. Mater.*, 2012, **24**, 115.

28 S. Kim, T. Y. Ohulchanskyy, H. E. Pudavar, R. K. Pandey and P. N. Prasad, Organically modified silica nanoparticles co-encapsulating photosensitizing drug and aggregation-enhanced two-photon absorbing fluorescent dye aggregates for two-photon photodynamic therapy, *J. Am. Chem. Soc.*, 2007, **129**, 2669.

29 J. E. Lee, N. Lee, H. Kim, J. Kim, S. H. Choi, J. H. Kim, T. Kim, I. C. Song, S. P. Park, W. K. Moon and T. Hyeon, Uniform mesoporous dye-doped silica nanoparticles decorated with multiple magnetite nanocrystals for simultaneous enhanced magnetic resonance imaging, fluorescence imaging, and drug delivery, *J. Am. Chem. Soc.*, 2010, **132**, 552.

30 P. Zrazhevskiy, M. Sena and X. Gao, Designing multifunctional quantum dots for bioimaging, detection, and drug delivery, *Chem. Soc. Rev.*, 2010, **39**, 4326.

31 Y. P. Ho and K. W. Leong, Quantum dot-based theranostics, *Nanoscale*, 2010, **2**, 60.

32 C. Liu, P. Zhang, X. Zhai, F. Tian, W. Li, J. Yang, Y. Liu, H. Wang, W. Wang and W. Liu, Nano-carrier for gene delivery and bioimaging based on carbon dots with PEI-passivation enhanced fluorescence, *Biomaterials*, 2012, **33**, 3604.

33 J. Zhang, L. Qiu, X. Li, Y. Jin and K. Zhu, Versatile preparation of fluorescent particles based on polyphosphazenes: from micro- to nanoscale, *Small*, 2007, **3**, 2081.

34 A. V. Kabanov, V. I. Slepnev, L. E. Kuznetsova, E. V. Batrakova, V. Yu. Alakhov, N. S. Melik-Nubarov, P. G. Sveshnikov and V. A. Kabanov, Pluronic micelles as a tool for low-molecular compound vector delivery into a cell: effect of Staphylococcus aureus enterotoxin B on cell loading with micelle incorporated fluorescent dye, *Biochem. Int.*, 1992, **26**, 1035.

35 D. Gyawali, S. Zhou, R. T. Tran, Y. Zhang, C. Liu, X. Bai and J. Yang, Fluorescence imaging enabled biodegradable photostable polymeric micelles, *Adv. Healthc. Mater.*, 2014, **3**, 182.

36 Y. Zhang, R. T. Tran, I. S. Qattan, Y. T. Tsai, L. Tang, C. Liu and J. Yang, Fluorescence imaging enabled urethane-doped citrate-based biodegradable elastomers, *Biomaterials*, 2013, **34**, 4048.

37 X. Feng, F. Lv, L. Liu, Q. Yang, S. Wang and G. C. Bazan, A highly emissive conjugated polyelectrolyte vector for gene delivery and transfection, *Adv. Mater.*, 2012, **24**, 5428.

38 Y. Sun, W. Cao, S. Li, S. Jin, K. Hu, L. Hu, Y. Huang, X. Gao, Y. Wu and X. J. Liang, Ultrabright and multicolorful fluorescence of amphiphilic polyethyleneimine polymer dots for efficiently combined imaging and therapy, *Sci. Rep.*, 2013, **3**, 3036.

39 M. F. Zambaux, F. Bonneaux, R. Gref, P. Maincent, E. Dellacherie, M. J. Alonso, P. Labrude and C. Vigneron, Influence of experimental parameters on the characteristics of poly(lactic acid) nanoparticles prepared by a double emulsion method, *J. Controlled Release*, 1998, **50**, 31.

40 L. E. Gerweck and K. Seetharaman, Cellular pH gradient in tumor versus normal tissue: potential exploitation for the treatment of cancer, *Cancer Res.*, 1996, **56**, 1194.

41 I. F. Tannock and D. Rotin, Acid pH in tumors and its potential for therapeutic exploitation, *Cancer Res.*, 1989, **49**, 4373.